nature communications

Article

https://doi.org/10.1038/s41467-025-58279-3

High-fidelity sub-microsecond single-shot electron spin readout above 3.5 K

Received: 15 June 2024

Accepted: 14 March 2025

Published online: 10 April 2025

Check for updates

H. Geng[1,2], M. Kiczynski[1,2], A. V. Timofeev[1,2], E. N. Osika[2], D. Keith[1,2], J. Rowlands[1], L. Kranz[1,2], R. Rahman[2], Y. Chung[1,2], J. G. Keizer[1,2], S. K. Gorman[1,2] & M. Y. Simmons[1,2]

Electron spin qubits in semiconductors are a promising platform for large-scale quantum computing due to their small size, long coherence and manufacturability. Typically, readout in spin qubits has been performed using energy-selective readout with extremely high fidelities up to 99.95% at millikelvin temperatures. Despite achieving record fidelities at low electron temperatures, the readout time remains on the order of 1 µs to 100 μs and comparable to the electron spin coherence time. In this paper we show that by engineering the location of two multi-donor quantum dot qubits with nanoscale precision we can demonstrate latched parity readout of two electrons in only 175 ns integration time with a fidelity of 99.44% at mK temperatures. Most importantly we show that this combination of strong confinement potential present in donor qubits with precision engineering of the tunnel rates allows us to operate our compact sensors at the highest temperatures recorded so far (3.7 K) using latched spin readout, giving a maximum fidelity of 97.87% in 1.5 μs. Our results demonstrate a clear performance improvement of state preparation and measurement using donor systems and offer the real possibility for operation of the surface-code using electron spins in semiconductor qubits.

Electron spin qubits controlled via ac electric[1,2] or magnetic[3,4] fields have shown tremendous progress in recent years. Single[2,5–7] and two-qubit[3,8–10] gate fidelities exceeding 99% have been demonstrated, along with greater than 99% fidelities in initialisation[11] and measurement[12–15]. With these milestones achieved, the field is now attempting to scale up qubit numbers while maintaining high-fidelity quantum operation[16–18]. A critical challenge for scale up is the cyrogenic cooling power needed to operate a large number of qubits. One of the significant advantages of semiconductor spin qubits is their robustness to high-temperature operation with single-qubit gates demonstrated above 1 K with a control fidelity of above 99%[19]. However at these high temperatures, the readout fidelity has been reduced to 60–95%[19–21]. The reduction in the readout fidelity was attributed to the reduced sensitivity of the single-electron transistor (SET) charge sensor at high-temperatures (>1 K) used in the experiments due to thermal broadening[21]. Despite this lower measurement fidelity, the promise of high-temperature operation opens up the possibility of adding classical control electronics alongside the quantum processor, thereby significantly decreasing the demands of cryogenic cooling.

Phosphorus-doped silicon quantum dot qubits and sensors are ideally suited for high-temperature operation. The phosphorus donor atoms provide a strong Coulomb confinement potential which gives rise to several advantages. First, the donor qubits themselves have a large orbital energy spacing, such that the excited states are far from the operable ground states (~5–10 meV), significantly increasing the operating temperature range for qubit control and readout[22]. The strong confinement also gives rise to SET charge sensors with large on-site energies (4–5 meV)[23] since these are also compact in size, around

[1]Centre of Excellence for Quantum Computation and Communication Technology, School of Physics, UNSW Sydney, Kensington, NSW, Australia. [2]Silicon Quantum Computing Pty Ltd, UNSW Sydney, Kensington, NSW, Australia. e-mail: michelle.simmons@unsw.edu.au

10x smaller than analogous sensors used in gate-based quantum dot devices[7,24]. Therefore a temperature increase from mK to~4 K, corresponding to approximately 0.4 meV, is around an order of magnitude less than the charging energy of the sensor, allowing for the electron occupation of the sensor to remain well-defined to high temperatures. Lastly, precision lithography[25] provides two additional advantages. The first is that it allows for the strongly confined quantum dots to be placed very close to the charge sensor (~10 nm) for fast operation, resulting in a large capacitive coupling, such that the strong-response regime of the SET charge sensor can be reached for maximum signal contrast[23]. The second is that the SET sensor can be precision engineered to maximise the ON/OFF ratio during charge detection. Here we can engineer a high conductance in the conducting/ON state where we can operate close to the quantum conductance limit with R_{SET} ~ 100 kΩ. In contrast in the insulating/OFF state, we operate deep in Coulomb blockade, where $R_{SET} > 10$ MΩ and we have a very low conductance. Combined this gives rise to the high ON/OFF contrast in our sensor response allowing both high temperature, and high fidelity spin read-out.

In this paper, we show how we can combine these benefits of Coulomb-confined phosphorus-doped silicon quantum dots with latched spin readout (LSR) to allow for fast, high-fidelity single-shot readout[12,26]. Since LSR only depends on charge tunnelling, it is less sensitive to thermal and external magnetic field constraints than traditional energy-selective spin readout[27]. This means we can engineer our SET charge sensors that are already strongly capacitively-coupled to be driven with more power, resulting in high signal-to-noise ratios (SNR), allowing us to operate at much higher temperatures (~3.7 K), compared to gate-defined quantum dots (~1.5 K)[19,21]. We show that at the mixing chamber base temperature of~0.02 K, we can achieve 99.44 ± 0.05% single-shot spin parity readout within only 175 ns integration time. We then compare our readout fidelities at 0.02 and 3.7 K where we show that the fidelity is only slightly reduced at high temperature due to the lower SNR of the SET. In both cases, we perform the experiments with an external magnetic field of 0.4 T. Through optimisation of the LSR parameters, we demonstrate single-shot spin parity readout of the electron spins at 3.7 K within 1.5 µs with a maximum readout fidelity of 97.87 ± 0.05%. These results demonstrate the possibilities for fast response phosphorus-doped silicon SET sensors that will allow high-temperature, large-scale quantum computing operation.

Results

To realise these results, we manufacture a double multi-donor quantum dot device using scanning tunnelling microscopy hydrogen resist lithography[25] in a natural silicon substrate as shown in Fig. 1a. In contrast to previously reported devices[22,25], the quantum dots in this LSR device are precision engineered such that they are asymmetrically tunnel coupled to the SET. We achieve this by increasing the relative geometric distance between one of the dots and the SET reservoir as can be seen in Fig. 1b, where the top dot (t) is around 10 nm further away from the SET compared to the bottom dot (b), strongly suppressing electron tunnelling to the top dot. The device is mounted on a custom printed circuit board (PCB) with the source contact connected to a RC bias-tee and rf-tank circuit. The rf-tank circuit consists of a $L_0 = 1.2$ µH inductor and $C_p = 0.4$ pF parasitic capacitance (giving a resonance frequency of f_r ~ 225 MHz) chosen to impedance match the SET with the 50 Ω transmission line to ensure maximum signal contrast[23]. This circuit probes the reflected input RF signal due to an admittance change of the rf-SET. The data from the device shown in this paper corresponds to a single rf-quadrature only, since the resonance frequency operating point is tuned such that the signal is maximised in one quadrature (Q) and minimised in the other (I). Figure 1c shows a 2D map of the reflected rf-signal as the left and right electrostatic gate voltages of the device are varied. The bright lines, running at 45°, correspond to where electrons tunnel through the SET causing a mostly dissipative response of the tank circuit (probing mostly rf-SET conductance)[23]. The distinct breaks in the rf-signal (dashed white lines), correspond to charge transitions of electrons between the two quantum dots and the electron reservoir. The charge states (n_b, n_t) corresponding to the number of electrons on the bottom (n_b) and top (n_t) quantum dots in each region are also shown in the figure.

There are two types of breaks or discontinuities in the stability diagram in Fig. 1c. In addition to the distinct shifts in SET response due to a change in total electron number, there are also small shifts or discontinuities at the (1,1) ↔ (2,0) region, highlighted by the green box, corresponding to the movement of an electron between the two quantum dots. These shifts are typically not observable in devices with symmetric dot-SET coupling[23]. Since the total number of electrons is conserved across this transition, the capacitive shift of the reflected signal from the SET charge sensor due to this electron movement is small. Here the movement of electrons between the quantum dots shifts the conductance peak by less than a full peak width (from blue to red) as illustrated in Fig. 1d, resulting in a readout contrast (difference in SET signal) that is <1. This is the operating regime for standard Pauli-spin blockade (PSB) readout[28]. To maximise the readout contrast, we can leverage the strong-response SET regime by performing LSR in the (2,1) charge region instead, where the total electron number of the system changes by 1. The addition and removal of a whole electron results in a much larger capacitive shift of the conductance signal during readout by a full peak width, as illustrated in Fig. 1e (blue box). In this case, there is maximum readout contrast of 1.

The 3-level pulse sequence for LSR is shown in Fig. 2a. First, the system is randomly initialised into one of the four, two-electron spin states ($|\uparrow\uparrow\rangle, |\uparrow\downarrow\rangle, |\downarrow\uparrow\rangle, |\downarrow\downarrow\rangle$) by pulsing from the (2,1) charge state to the (1,1) charge region at point **A** where the two electrons are weakly interacting. Next, the system is pulsed to point **B** in the (2,0) charge region where now due to the presence of the exchange interaction between the two donor dots, the two spin basis states form the singlet (S: $|\uparrow\downarrow\rangle - |\downarrow\uparrow\rangle$) and triplet ($T_0$: $|\uparrow\downarrow\rangle + |\downarrow\uparrow\rangle$, T_+: $|\uparrow\uparrow\rangle$, T_-: $|\downarrow\downarrow\rangle$) states. The pulse from **A** → **B** passes through the $S - T_-$ anti-crossing, hence the finite rise time (~1 ns) of the arbitrary waveform generator used to generate the pulse results in a small adiabatic loss (~0.07%), as calculated by the Landau–Zener formula. The time spent at point **B** is short, such that the even parity states do not have enough time to relax to the (2,0) charge ground state, but long enough that the singlet-triplet (T_0) states mix together due to the strong hyperfine coupling present in donor devices[29]. Hence at point **B** the even parity states ($|\uparrow\uparrow\rangle, |\downarrow\downarrow\rangle$) remain in the (1,1) charge configuration due to Pauli spin blockade. Meanwhile the odd parity spin states form the singlet-triplet (T_0) states ($|\uparrow\downarrow \pm \downarrow\uparrow\rangle$) in the (2,0) region where both electrons are on dot b. Pauli spin blockade is lifted for the odd states, allowing these states to occupy the (2,0) charge configuration. Lastly, latched readout is performed by pulsing to point **C** in the (2,1) charge region and waiting for a settling time of 250 ns before integrating the SET signal. This settling time leads results in ~0.47% of the odd states relaxing to the even states in this period of time. Here, as shown by the orange section of the energy level diagram in Fig. 2b, an even parity state maps directly to the (2,1) charge configuration while an odd parity state is initially latched to the (2,0) charge state, due to the slow tunnel rate between the charge states (2,0) ↔ (2,1) that has been engineered by moving the dot further away from the SET sensor, as illustrated in Fig. 1b. By biasing the readout position to the top of a conductance peak in the (2,1) region, we observe in Fig. 2c that the SET charge sensor trace produced by the even state (blue) remains high throughout the measurement period. While the odd state (red) starts with a low trace that becomes high as it relaxes to the ground state (dashed arrow in Fig. 2b).

The parity-based readout can also be used for readout of an individual spin qubit (top quantum dot) via coupling to the ancilla

https://doi.org/10.1038/s41467-025-58279-3

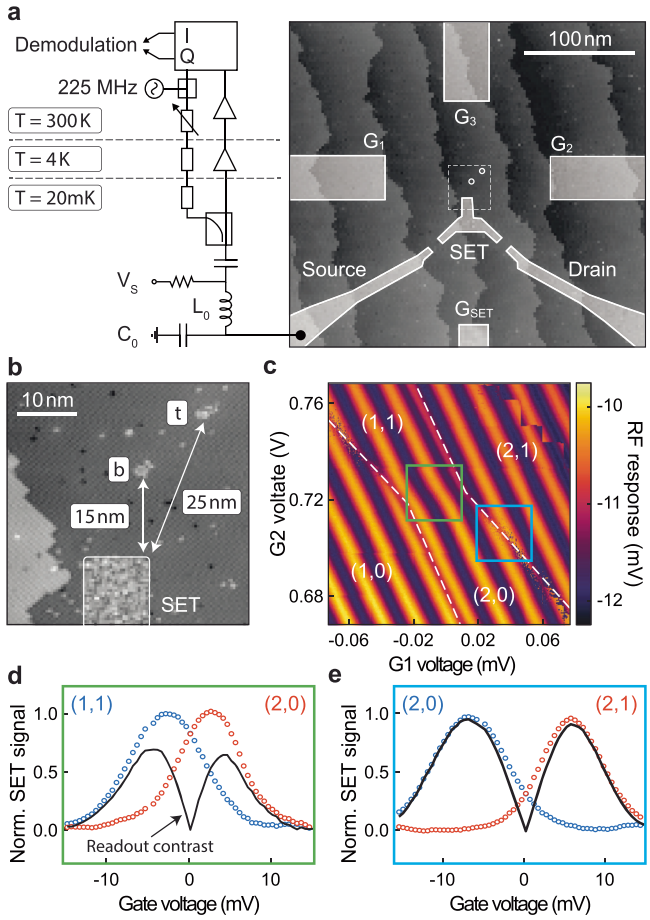

Fig. 1 | High-fidelity singlet-triplet spin readout in a double donor quantum dot using a latched readout mechanism. a Scanning-tunnelling micrograph of the device used in this paper along with measurement schematic. The bright regions correspond to bare silicon bonds where the atomic hydrogen mask has been removed to define the quantum dots, single-electron transistor (SET) and control gates. The SET was measured using a resonant *LC* tank circuit as described in the main text. **b** Enlarged image of the quantum dots (*t* and *b*) and the top of the SET charge sensor. **c** A single rf-quadrature response (arbitrary units) of the SET as a function of the left and right gate voltages with the quantum dot charge regions shown as (n_b, n_t). Two different tunnelling processes can be detected by the SET: **d** The movement of an electron between the quantum dots (green box in **c**) which only shifts the conductance peak of the SET by a small amount, from the blue to the red peak. The black line indicates the readout contrast as the absolute difference between the two SET signals. **e** The tunnelling of an electron from the quantum dots to the SET reservoir (blue box in **c**) where the shift of the conductance peak is greater than a full peak width, hence there is maximum readout contrast.

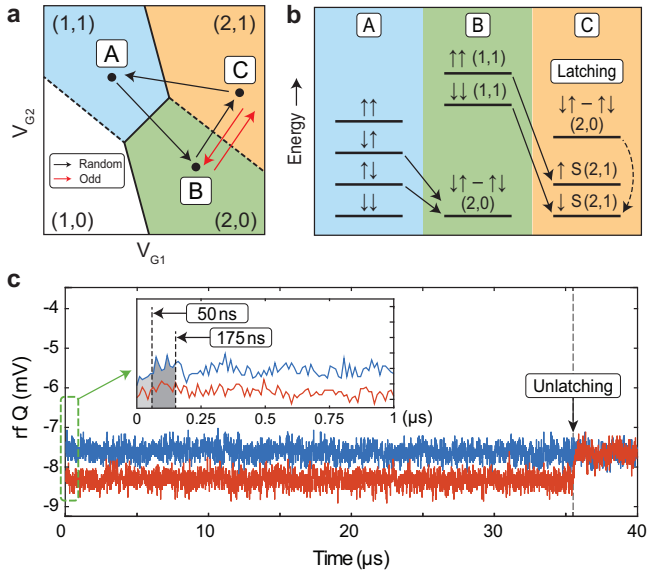

Fig. 2 | Latched readout in engineered donor quantum dots. a Schematic of the charge stability diagram showing the 3-level pulse sequence used to perform latched spin readout on a random spin state (black) and to deterministically load an odd state (red). **b** The illustrative energy level diagram at each of the 3 points in the readout pulse sequence. Solid arrows indicate a direct mapping while the dashed arrow represents a slower relaxation process. **c** Example SET charge sensor traces showing the signal for odd parity (red) and even parity (blue) states where the readout position is biased to the top of Coulomb peak in the (2,1) region. Inset shows the signal at times<1 μs and where the shaded regions of 50 and 175 ns correspond to the integration windows used for the fidelity analysis.

(bottom quantum dot loaded deterministically with a down electron). The high signal contrast observed arises due to the addition of a whole electron with associated large capacitive shift of the charge sensor, allowing for high-fidelity readout[12]. While we focus on characterising the fidelity to discriminate between parity states, in principle, we could extend the analysis to include other aspects required for the fidelity of the individual qubit readout relevant for quantum error correction. However, this would involve determining additional experimental parameters such as electron spin resonance efficiency and initialisation fidelity for each electron spin which we could not measure in this device without the use of isotopically pure Si-28 and the addition of an on-chip microwave antenna for magnetic drive.

Latched spin readout offers two main advantages over energy-selective measurements (ESM)[30,31]: high-temperature operation and non-stochastic tunnel events. Energy-selective readout relies on the spin qubit energy being much larger than the temperature of the system which typically limits the operating temperature to be ≪1 K[32] for qubit energies of ~20–40 GHz[6,33]. The lower thermal constraints on LSR also mean more power can be applied to the readout sensor, further increasing the readout signal. Additionally, ESM inherently involves stochastic tunnelling processes such that the sensor signal cannot be filtered using standard integration filters[32], thus ultimately lowering the maximum achievable readout fidelity. On the other hand, for LSR, the SET signal begins in the desired measurable state, either even or odd (see Fig. 2c), hence the measurement window can be applied straight away, reducing the integration time needed. Finally, since LSR directly measures the two-spin state we can use it to characterise the tunnel coupling, t_c between quantum dots via a spin-funnel measurement by plotting the detuning position of the S–T minus anti-crossing[34]. For this device we find t_c = 3 GHz at 0.02 K with an estimated gradient magnetic field of ~50 MHz shown in Supplementary I[25].

Ultimately, the fidelity of LSR strongly depends on the tunnelling transport characteristics of the SET and how it varies with temperature. In Fig. 3a we show the SET signal as a function of gate voltage while the bath temperature of the dilution refrigerator was varied from 0.1 K to 3.7 K, while keeping the rf signal constant. The SET signal peak height does not vary considerably even up to 3.7 K. Here, the tank circuit is being driven at high rf-power, already effectively power-broadening the SET response. This power-broadening only weakly affects the LSR fidelity (due to the strong capacitive coupling of the quantum dot to the SET which shifts the signal by a full peak width) and hence we can operate in the power-broadened regime for all temperatures[26].

For readout in the strong response regime[23], we are most interested in the change in peak height since we operate at the maximum signal point and not the maximum sensitivity point. To further illustrate this we plot the measured SET signal, $V_{contrast} = \max(V_Q) - \min(V_Q)$ in Fig. 3b. The maximum SET signal of 0.7 mV is maintained up to ~1 K, and then drops to only half of its maximum value (0.35 mV) as the temperature is increased to 3.7 K. As the readout speed is critical

https://doi.org/10.1038/s41467-025-58279-3

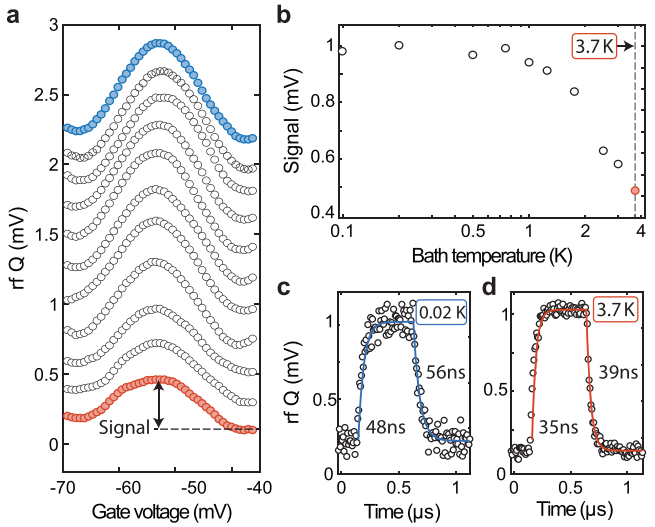

Fig. 3 | Single-electron transistor charge sensor performance as a function of temperature. a Measurement of a single conductance peak (rf quadrature signal) as a function of bath temperature from 0.1 K (blue) to 3.7 K (red). Each trace is offset by 0.15 mV. **b** The corresponding normalised signal of the SET (maximum signal−minimum signal) from the conductance peaks in (**a**). The SET performance remains constant up to ~1 K and then drops quickly above 1 K. **c** The response time of the SET at 0.02 K and **d** 3.7 K by fitting to the normalised signal of the SET when applying a 500 ns square pulse. At both temperatures, we find exponential response times~50 ns.

for large-scale quantum processors, we also performed temporal measurements of the rf-SET tank circuit transient response at 0.02 and 3.7 K by applying 500 ns square pulses to one of the electrostatic gates between lifted and full Coulomb blockade as shown in Fig. 3c, d. By fitting exponential transients of the average rf-SET response, we find the characteristic (1/*e*) rise–fall constants to be $\tau_{0.02K} = 48–56$ ns and $\tau_{3.7K} = 35–39$ ns corresponding to quality factors ($Q = 2\pi f_r \tau$) of $Q = 34–39$ at 0.02 K and $Q = 25–27$ at 3.7 K. These Q-factors are comparable to previously reported values in phosphorus-doped silicon[23] allowing for high measurement bandwidths. The signal contrast and speed can be improved with further improvements in the readout circuit setup. The noise in the system is currently limited by the cold preamplifier[23], such that the signal contrast can be further increased by using lower noise parametric cold amplifier[35,36]. The speed can be increased by optimising the resonant circuit to have a higher resonance frequency (f_{res}) while maintaining the same quality factor (Q) as the bandwidth is f_{res}/Q.

Now that we have established the performance of the SET as a function of temperature, we demonstrate LSR at the mixing chamber base temperature of 0.02 K and at 3.7 K to investigate the low-temperature and high-temperature single-shot spin readout fidelity. In Fig. 4a we show the measured parity readout error (1 − fidelity) as a function of integration time (using a boxcar filter) of the SET signal at 0.02 and 3.7 K by fitting to the equations described in Barthel et al.[37], see Supplementary II. The model takes into account the unlatching of the (2,0) odd state to the (2,1) charge state due to an electron tunnelling from the reservoir to the top dot (t) during the integration period. This can be seen as the relaxation of the odd state with a T_1 time

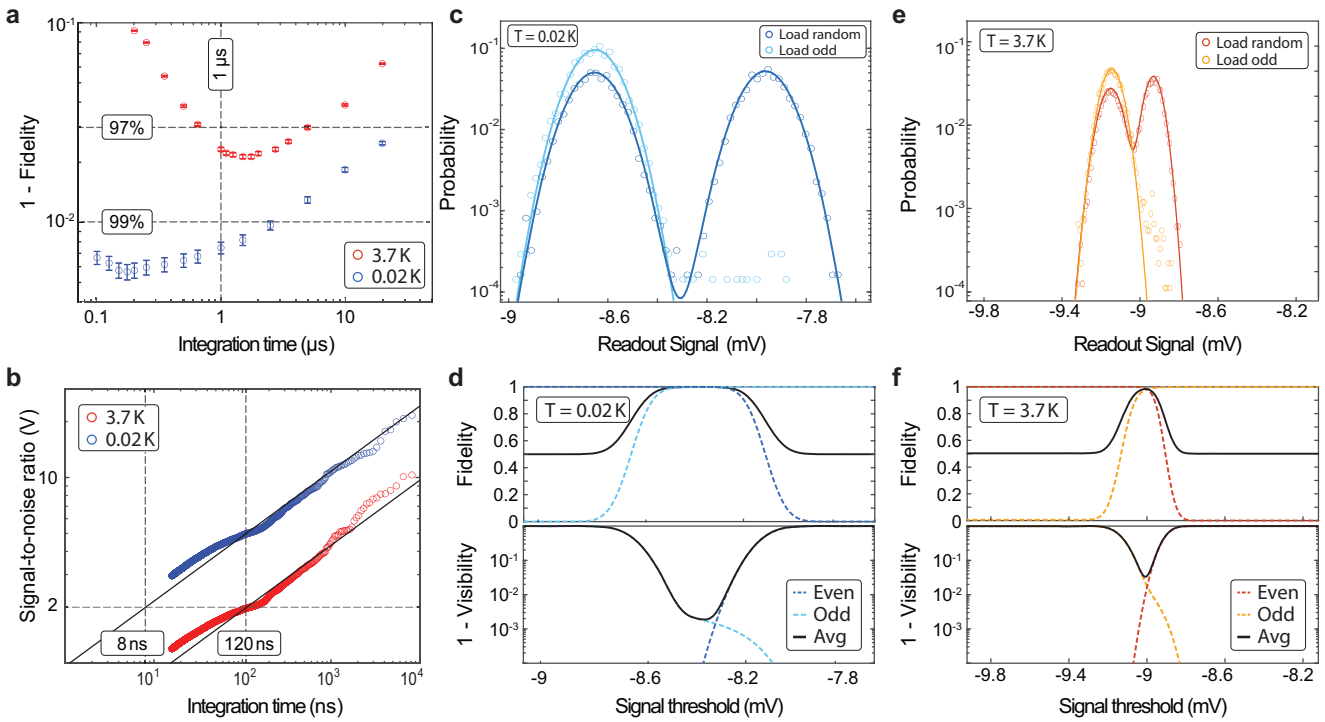

Fig. 4 | High-fidelity single-shot electron spin readout above 3.5 K. a The spin readout (1 − fidelity) as a function of integration time of the SET signal at 0.02 K (blue circles) and 3.7 K (red circles). For short integration times the fidelity is limited by electrical noise from the amplification chain. For longer integration times the signal-to-noise ratio (SNR) is limited by the decay of the odd state to the (2,1) state. Error bars represent 1 standard deviation. **b** The SNR as a function of integration time of the SET signal. The lines represent linear extrapolations (on a log-scale) to estimate the measurement time, τ_m of the SET at 0.02 and 3.7 K. We can see that τ_m is significantly reduced by decreasing the operation temperature. **c** The signal histograms for detecting odd and even states for an integration time of 175 ns at 0.02 K. **d** The fidelity and (1 − visibility) of each odd parity and even parity state as a function of the threshold value of the integrated signal. The large separation between the two peaks corresponds to a maximum readout fidelity of 99.44%. **e** The same as (**c**) but for 3.7 K with 1.5 μs integration time. **f** The same as in (**d**) but for 3.7 K operation temperature. The maximum readout fidelity is only slightly reduced to 97.87% at the much higher operation temperature.

of 53 ± 1 µs at 0.02 K and 53 ± 2 µs at 3.7 K, extracted from the average odd parity RF signal shown in Supplementary III. Since it is a tunnelling process, it is not dominated by the temperature of the system in the experiments and therefore remains consistent as the temperature is increased. For short integration times, the fidelity is limited by the signal-to-noise ratio (SNR) of the SET in which the cold (HEMT) pre-amplifier noise dominates the signal[23]. For longer integration times the tunnelling induced relaxation rate of the (2,0) odd parity states into the (2,1) charge state begins to dominate the fidelity and leads to an exponential increase in readout error seen in Fig. 4a. The optimal integration time is, therefore, a trade-off between these two effects: SNR and relaxation. The fidelity is significantly better at 0.02 K than at 3.7 K for short integration times due to the lower SET signal at higher temperatures. For integration times longer than 1 μs, the fidelities at both temperatures begin to approach each other. This is due to the fact that in this regime, relaxation errors dominate, and the measured relaxation time of the singlet at 3.7 K (~53 µs) is the same as the relaxation time at 0.02 K. Therefore, the main difference in the readout fidelities at the two temperatures is simply due to the SNR of the SET.

The SNR of the SET is plotted as a function of integration time at 0.02 and 3.7 K in Fig. 4b. We can see that the SNR values of the SET is significantly larger at 0.02 K compared to 3.7 K for any given integration time as expected from the decrease in the size of the SET signal peak measured in Fig. 3b. From extrapolating the SNR values vs integration time for both temperatures, we can estimate the measurement time τ_m of the sensor, defined as the integration time required to achieve a SNR of 2[38]. Separate to the integration time, the measurement time is a metric that accounts for the noise and bandwidth of the charge sensor, giving an indication of the quality, and should be as short as possible for high-fidelity readout. Here, we measure $\tau_m = 8 \pm 1.5$ ns (0.02 K) and $\tau_m = 120 \pm 12$ ns (3.7 K). At elevated temperatures of 3.7 K, the phosphorus-doped silicon SET still acts as a high contrast, fast charge sensor.

The maximum fidelity at 0.02 K was calculated to be 99.44 ± 0.05% with an integration time of 175 ns with the signal histogram (dark blue) shown in Fig. 4c. As we wait 250 ns settling time, the total measurement time is 425 ns and we have accounted for spin relaxation in the fidelity over this total period. We load 6000 random states (at point A in Fig. 2a) with single-shot readout traces taken, resulting in two equal-sized probability peaks corresponding to both the odd and even states. We can deterministically load an odd state by waiting longer at point B in Fig. 2a where an even state will relax to the lower energy odd state. This results in a single peak, as illustrated by the light blue signal histogram overlaid. The latched parity readout error at 0.02 K (0.5%) is half the 1% fault-tolerant threshold and 3 orders of magnitude faster than the longest reported dephasing time (270 µs[6]) for an electron spin qubit using phosphorus-doped silicon. These readout metrics are comparable to the fastest recorded superconducting qubit readout times[39,40] and faster than the highest reported times for spin qubits (99% at 1.6 µs[41]) while demonstrating one of the highest fidelities to date. In Fig. 4d we show the fidelity as a function of the signal threshold which is defined as the level at which any signal above is classified as an even state and any signal below is an odd state. High-fidelity readout was maintained while decreasing the integration times further, with 99.15% achieved at the minimum measured integration time of 50 ns.

At 3.7 K, the maximum readout fidelity obtained was 97.87 ± 0.05% in 1.5 µs. Figure 4e shows the optimal measured signal histogram for latched readout (red) where we can see the asymmetry in the peaks due to the relaxation of the singlet state and the histogram for deterministically loaded odd states (orange) where only one peak is visible, as expected. In Fig. 4f, we plot the individual state fidelities as a function of the threshold voltage used to distinguish the two histograms. Compared to 0.02 K we find a reduction of only less than 2% fidelity when operating the device at 3.7 K. This fidelity is currently limited by the SNR of the charge sensor which can be increased further by better amplification of the SET signal and additional optimisation of the SET tunnel junctions to increase conductance, which if implemented in the future, can help push high temperature latched readout fidelity above the fault tolerant threshold of 99%. The current readout fidelity obtained at 3.7 K also implies that temperatures above 1 K (where the use of a dilution unit is not required) should be readily achievable for qubit readout above 99% allowing for high-temperature qubit operation.

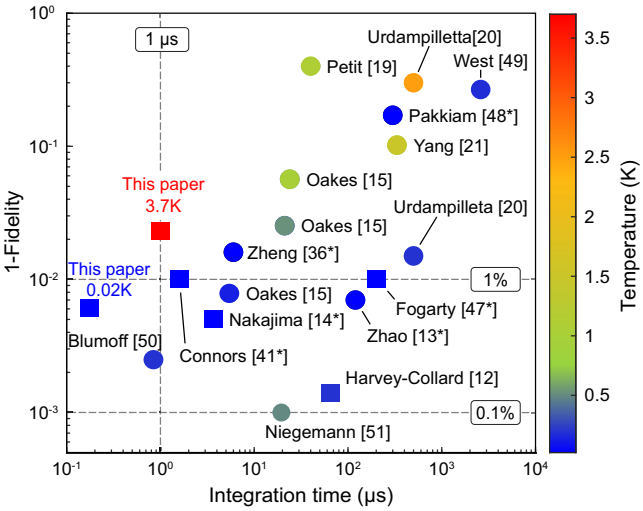

Fig. 5 | Comparison of fidelity and speed of Pauli-spin blockade-based readout. Experimentally measured fidelity and integration times, published in the literature[12–15,19–21,36,41,47–51], for Pauli-spin blockade-based readout at different electron temperatures. Square markers correspond to readout utilising the latched mechanism and circle markers are results obtained using non-latched readout. Markers with an asterisk indicate results obtained at base dilution fridge temperatures, where the electron temperature was not explicitly stated.

Discussion

These results represent a significant improvement over previous spin readout experiments in terms of speed and temperature as shown in Fig. 5, where results from this paper and previously published experimental results are plotted. Readout experiments utilising LSR are depicted by squares, while non-latched readout experiments are shown as circles. It can be seen in Fig. 5 that the use of LSR in qubit systems has generally increased spin readout fidelities over non-latched methods, reaching and exceeding the 99% threshold required for fault-tolerant quantum computation[42]. Also due to the greater signal contrast, LSR has shortened the integration time necessary to obtain high fidelity readout. Hence, by combining a strongly coupled SET with asymmetric engineering of dot-to-reservoir tunnel rates to enable LSR, we have been able to achieve sub-microsecond readout with a fidelity of over 99.4%. Using this method, we were also able to obtain higher fidelity and faster readout, at a much higher temperature (red square) than achieved in previous works. Our high-temperature results, with a shorter integration time, even compare favourably in terms of fidelity to results obtained at millikelvin temperatures in other systems.

In summary, we have demonstrated 99.44 ± 0.05% single-shot spin readout fidelity at 0.02 K temperatures with an integration time of 175 ns by leveraging the strong confinement of donor-based quantum dots to engineer a large SET signal. We have shown that the strong SET signal is maintained for temperatures up to 1 K with fidelity of 97.87 ± 0.05 % at 3.7 K. Whilst a disadvantage of SET sensors is that they require 3 terminals with a sizable physical footprint (~900 nm^2) this is still much smaller than comparable sensors found in gate-based

quantum dot devices (~10,000 nm^2)[7,24]. Recent work has shown however that we can create even smaller (~150 nm^2) single lead sensors[43] using donor-based quantum dots of similar size and can manufacture the SET in three dimensions[44], to allow for a scalable surface code architecture[45]. These results demonstrate the benefit of LSR combined with the strong response regime available in donor-based systems to achieve high-fidelity readout with the prospect of operating large-scale quantum processors without requiring a dilution refrigerator[46]. In the future, the use of isotopically purified silicon-28 growth for high-fidelity qubit control and on-chip antenna will be used to independently quantify qubit visibility via rabi oscillations.

Data availability

Source data are provided upon request from the corresponding author.

References

1. Watson, T. F. et al. A programmable two-qubit quantum processor in silicon. *Nature* **555**, 633 (2018).
2. Zajac, D. M. et al. Resonantly driven CNOT gate for electron spins. *Science* **359**, 439 (2018).
3. Madzik, M. T. et al. Precision tomography of a three-qubit donor quantum processor in silicon. *Nature* **601**, 348 (2022).
4. Evans, T. et al. Fast Bayesian tomography of a two-qubit gate set in silicon. *Phys. Rev. Appl.* **17**, 024068 (2022).
5. Veldhorst, M. et al. An addressable quantum dot qubit with fault-tolerant control fidelity. *Nat. Nanotechnol.* **9**, 981 (2014).
6. Muhonen, J. T. et al. Storing quantum information for 30 seconds in a nanoelectronic device. *Nat. Nanotechnol.* **9**, 986 (2014).
7. Yoneda, J. et al. A quantum-dot spin qubit with coherence limited by charge noise and fidelity higher than 99.9%. *Nat. Nanotechnol.* **13**, 102 (2018).
8. Noiri, A. et al. Fast universal quantum gate above the fault-tolerance threshold in silicon. *Nature* **601**, 338 (2022).
9. Xue, X. et al. Quantum logic with spin qubits crossing the surface code threshold. *Nature* **601**, 343 (2022).
10. Mills, A. R. et al. Two-qubit silicon quantum processor with operation fidelity exceeding 99%. *Sci. Adv.* **8**, eabn5130 (2022).
11. Watson, T. F., Weber, B., House, M. G., Büch, H. & Simmons, M. Y. High-fidelity rapid initialization and read-out of an electron spin via the single donor D^- charge state. *Phys. Rev. Lett.* **115**, 166806 (2015).
12. Harvey-Collard, P. et al. High-fidelity single-shot readout for a spin qubit via an enhanced latching mechanism. *Phys. Rev. X* **8**, 021046 (2018).
13. Zhao, R. et al. Single-spin qubits in isotopically enriched silicon at low magnetic field. *Nat. Commun.* **10**, 1 (2019).
14. Nakajima, M. R. et al. Robust single-shot spin measurement with 99.5% fidelity in a quantum dot array. *Phys. Rev. Lett.* **119**, 017701 (2017).
15. Oakes, G. et al. Fast high-fidelity single-shot readout of spins in silicon using a single-electron box. *Phys. Rev. X* **13**, 011023 (2023).
16. Philips, S. G. J. et al. Universal control of a six-qubit quantum processor in silicon. *Nature* **609**, 919 (2022).
17. Weinstein, A. J. et al. Universal logic with encoded spin qubits in silicon. *Nature* **615**, 817 (2023).
18. Takeda, K., Noiri, A., Nakajima, T., Kobayashi, T. & Tarucha, S. Quantum error correction with silicon spin qubits. *Nature* **608**, 682 (2022).
19. Petit, L. et al. Universal quantum logic in hot silicon qubits. *Nature* **580**, 355 (2020).
20. Urdampilleta, M. et al. Gate-based high fidelity spin readout in a CMOS device. *Nat. Nanotechnol.* **14**, 737 (2019).
21. Yang, C. H. et al. Operation of a silicon quantum processor unit cell above one kelvin. *Nature* **580**, 350 (2020).
22. Broome, M. A. et al. Two-electron spin correlations in precision placed donors in silicon. *Nat. Commun.* **9**, 980 (2018).
23. Keith, D. et al. Single-shot spin readout in semiconductors near the shot-noise sensitivity limit. *Phys. Rev. X* **9**, 041003 (2019).
24. Nichol, J. M. et al. High-fidelity entangling gate for double-quantum-dot spin qubits. *npj Quantum Inf.* **3**, 3 (2017).
25. He, Y. et al. A two-qubit gate between phosphorus donor electrons in silicon. *Nature* **571**, 371 (2019).
26. Osika, E. N. et al. Shelving and latching spin readout in atom qubits in silicon. *Phys. Rev. B* **106**, 075418 (2022).
27. Elzerman, J. et al. Single-shot read-out of an individual electron spin in a quantum dot. *Nature* **430**, 431 (2004).
28. Petta, J. R. et al. Coherent manipulation of coupled electron spins in semiconductor quantum dots. *Science* **309**, 2180 (2005).
29. Barthel, C. et al. Relaxation and readout visibility of a singlet-triplet qubit in an Overhauser field gradient. *Phys. Rev. B* **85**, 035306 (2012).
30. Elzerman, J. M. et al. Single-shot read-out of an individual electron spin in a quantum dot. *Nature* **430**, 431 (2004).
31. Keith, D. et al. Ramped measurement technique for robust high-fidelity spin qubit readout. *Sci. Adv.* **8**, eabq0455 (2022).
32. Keith, D. et al. Benchmarking high fidelity single-shot readout of semiconductor qubits. *N. J. Phys.* **21**, 063011 (2019).
33. Fricke, L. et al. Coherent control of a donor-molecule electron spin qubit in silicon. *Nat. Commun.* **12**, 1 (2021).
34. Maune, B. M. et al. Coherent singlet-triplet oscillations in a silicon-based double quantum dot. *Nature* **481**, 344 (2012).
35. Schaal, S. et al. Fast gate-based readout of silicon quantum dots using Josephson parametric amplification. *Phys. Rev. Lett.* **124**, 067701 (2020).
36. Zheng, G. et al. Rapid gate-based spin read-out in silicon using an on-chip resonator. *Nat. Nanotechnol.* **14**, 742 (2019).
37. Barthel, C., Reilly, D. J., Marcus, C. M., Hanson, M. P. & Gossard, A. C. Rapid single-shot measurement of a singlet-triplet qubit. *Phys. Rev. Lett.* **103**, 160503 (2009).
38. Makhlin, Y., Schön, G. & Shnirman, A. Quantum-state engineering with Josephson-junction devices. *Rev. Mod. Phys.* **73**, 357 (2001).
39. Sunada, Y. et al. Fast readout and reset of a superconducting qubit coupled to a resonator with an intrinsic Purcell filter. *Phys. Rev. Appl.* **17**, 044016 (2022).
40. Heinsoo, J. et al. Rapid high-fidelity multiplexed readout of superconducting qubits. *Phys. Rev. Appl.* **10**, 034040 (2018).
41. Connors, E. J., Nelson, J. J. & Nichol, J. M. Rapid high-fidelity spin state readout in Si/Si-Ge quantum dots via rf reflectometry. *Phys. Rev. Appl.* **13**, 024019 (2020).
42. Fowler, A. G., Mariantoni, M., Martinis, J. M. & Cleland, A. N. Surface codes: Towards practical large-scale quantum computation. *Phys. Rev. A* **86**, 032324 (2012).
43. Hogg, M. R. et al. Single-shot readout of multiple donor electron spins with a gate-based sensor. *PRX Quantum* **4**, 010319 (2023).
44. Koch, M. et al. Spin read-out in atomic qubits in an all-epitaxial three-dimensional transistor. *Nat. Nanotechnol.* **14**, 137 (2019).
45. Hill, C. D. et al. A surface code quantum computer in silicon. *Sci. Adv.* **1**, e1500707 (2015).
46. Vandersypen, L. M. K. et al. Interfacing spin qubits in quantum dots and donors—hot, dense, and coherent. *npj Quantum Inf.* **3**, 34 (2017).
47. Fogarty, M. A. et al. Integrated silicon qubit platform with single-spin addressability, exchange control and single-shot singlet-triplet readout. *Nat. Commun.* **9**, 4370 (2018).
48. Pakkiam, P. et al. Single-shot single-gate RF spin readout in silicon. *Phys. Rev. X* **8**, 041032 (2018).
49. West, A. et al. Gate-based single-shot readout of spins in silicon. *Nat. Nanotechnol.* **14**, 437 (2019).

50. Blumoff, J. Z. et al. Fast and high-fidelity state preparation and measurement in triple-quantum-dot spin qubits. *PRX Quantum* **3**, 010352 (2022).
51. Niegemann, D. J. et al. Parity and singlet-triplet high-fidelity readout in a silicon double quantum dot at 0.5 k. *PRX Quantum* **3**, 040335 (2022).

Acknowledgements

This research is supported by Silicon Quantum Computing Pty Ltd., the Australian Research Council Centre of Excellence for Quantum Computation and Communication Technology (Project no. CE110001027). M.Y.S. acknowledges an Australian Research Council Laureate Fellowship.

Author contributions

H.G., M.K., and J.R. fabricated the device under the supervision of Y.C. and J.G.K., H.G., M.K., A.V.T., and S.K.G. measured the device. H.G., A.V.T., D.K., and S.K.G. analysed the data. E.N.O. assisted with theoretical calculations under the supervision of R.R. The manuscript was written by H.G., A.V.T., L.K., S.K.G, and M.Y.S. with input from all authors. S.K.G. and M.Y.S. supervised the project.

Competing interests

M.Y.S. is the CEO and director of the company Silicon Quantum Computing Pty Ltd. H.G., M.K., A.V.T., E.N.O., D.K., J.R., L.K., R.R., Y.C., J.G.K., S.K.G., and M.Y.S. (all authors) declare equity interest in Silicon Quantum Computing Pty Ltd.

Additional information

Supplementary information The online version contains supplementary material available at https://doi.org/10.1038/s41467-025-58279-3.

Correspondence and requests for materials should be addressed to M. Y. Simmons.

Peer review information *Nature Communications* thanks Yutaka Tabuchi, Matias Urdampilleta, and the other, anonymous, reviewers for their contribution to the peer review of this work. A peer review file is available.